ROYAL SOCIETY OF CHEMISTRY

PAPER

Check for updates

Dry reforming of methane over Co–Mo/Al2O3 catalyst under low microwave power irradiation†

Hoang M. Nguyen, [iD] [a] Gia Hung Pham,*[a] Ran Ran,[a] Robert Vagnoni,[b] Vishnu Pareek[a] and Shaomin Liu [iD] *[a]

In this work, microwave (MW) irradiation was used to activate Co/Al_2O_3, Mo/Al_2O_3, and $Co–Mo/Al_2O_3$ catalysts for dry reforming of methane (DRM) reactions. Experimental results indicate that single metallic catalysts of either Co or Mo are inactive for DRM under all the tested conditions due to their limited MW-absorbing ability. In contrast, Co–Mo bimetallic catalysts supported by Al_2O_3 exhibit high catalytic activity due to the formation of a magnetodielectric $Co_{0.82}Mo_{0.18}$ alloy, which plays the dual role of a good MW acceptor and the provider of active centers for the DRM reaction. The MW power level required to activate such bimetallic catalysts for DRM is significantly dependent on the molar ratio between Co and Mo. The CoMo2 catalyst (with a molar ratio of 2.0 Co to 1.0 Mo) supported on Al_2O_3 exhibits the best catalytic performance, converting 80% CH_4 and 93% CO_2 to syngas at a ratio of H_2/CO of 0.80 at the total volumetric hourly space velocity (VHSV) of 10 L g^{-1} h^{-1} and MW power of 200 W. As compared to the reported C-based catalysts, the $Co–Mo/Al_2O_3$ catalyst delivers more favorable stability over 16 time-on-stream (TOS) by virtue of its intrinsic ability to absorb MW without the inclusion of auxiliary MW acceptors.

1. Introduction

A growing share of the world's natural gas reserves is located in remote areas like deep offshore, of which relatively bigger gas reserves can be harnessed by liquefying the natural gas (LNG) for transportation using tanks. However, most of the small gas reserves are stranded: in the case of associated production (*i.e.*, gas produced with crude oil), the natural gas has to be re-injected.[1–3] This not only results in the loss of income but also pollutes the environment due to gas leakage to air. Because of this, there is a sustained demand for small-to-medium-sized gas-to-liquid (GTL) plants on floating production, storage, and offloading vessels (FPSOVs). These are particularly important for small stranded gas reserves, where the gas pipeline option is completely uneconomical. The production of syngas is the first step in a GTL plant, which must have the minimal weight to be suitable for FPSOVs.

Among the three methane reforming methods (dry, steam, and autothermal), dry reforming of methane (DRM) has attracted increased attention due to the conversion of two greenhouse gases (CH_4, CO_2) to produce syngas (H_2 and CO), which is used as the feed for Fischer–Tropsch synthesis.[4] The

primary challenge in the applications of the DRM process is the thermodynamic barrier caused by the high thermal stability of CH_4 and CO_2 requiring higher temperatures (700–1200 °C) for the DRM operation to achieve expected conversions.[5] Most of the current studies on DRM have used conventional electric heating methods,[6] which not only consume considerable energy but also require heavy heat exchanger tubes, complicating the operation of a reformer system in FPSOV vessels.[2] Microwave (MW) is known to be an energy-saving heating method, which can be used to reduce energy consumption for DRM processes.[7] Other advantages of using the MW heating system are greater control over the heating process, quick start and stop facility, and high level of safety and automation.[8] Prominently, DRM heated by MW irradiation allows to reduce the number of equipment, which favors the riser and mooring systems to produce syngas and imparts greater flexibility in controlling the reactor size through which a lightweight reformer can be fabricated, particularly for FPSOVs. MW plasma DRM reaction without a catalyst has been investigated by several researchers.[9–11] However, plasma processes have low energy efficiency owing to the higher MW power required to stabilize plasma.[12] In order to effectively reduce the energy consumption, a combination of catalyst and MW irradiation is considered to be a promising approach. The primary idea of combining MW and heterogeneous catalysis is to exert volumetric controllable electromagnetic action on the catalyst–reagents system. This action alters the state of the reaction system and leads to a

[a] *Department of Chemical Engineering, Curtin University, GPO Box U1987, Perth, Western Australia, 6845, Australia. E-mail: G.Pham@curtin.edu.au, Shaomin.Liu@curtin.edu.au*

[b] *Eco Technol Co., Pty Ltd, Perth, Western Australia, 6009, Australia*

† Electronic supplementary information (ESI) available. See DOI: 10.1039/c8cy01601a

This journal is © The Royal Society of Chemistry 2018

Catal. Sci. Technol., 2018, **8**, 5315–5324 | 5315

considerable change in the apparent thermodynamics of the gas-phase reactions, resulting in higher conversion values at lesser extreme conditions.[13] A catalytic DRM process under MW irradiation can compete with currently well-established steam-based methane reforming processes in terms of conversion amounts and energy consumption.[14] All the reported works on DRM under MW heating simply used carbon-based materials as the catalyst[15–19] since carbon-based materials are good MW absorbers. However, the catalytic activity and stability of carbon-based catalysts deteriorate significantly due to carbon loss.[20] Consequently, there is a room for the development of catalysts for DRM heated by MW irradiation.

Co is known to be a good catalyst/promoter of reforming reactions.[21–24] Coke deposition, which leads to catalyst deactivation, is one of the main constraints of Co-based catalysts.[25] Mo is considered as an environmentally friendly and cost-effective catalyst with longstanding stability toward hydrogenating reactions.[26] Hence, the addition of Mo in the Co/Al_2O_3 structure suppresses coke deposition during the reforming process.[27] In the literature, Co/Al_2O_3 (ref. 28 and 29) and Mo/Al_2O_3 (ref. 30) catalysts exhibit catalytic activity for DRM under conventional heating. Meanwhile, Co–Mo/Al_2O_3 has been extensively investigated as an efficient catalyst for several processes such as hydrodesulfurization,[31–34] hydrotreatment,[35,36] syngas conversion,[37] and natural gas decomposition.[27] Nonetheless, a highly efficient Co–Mo/Al_2O_3 catalyst for DRM, particularly under MW irradiation, has not been reported. The main objective of this work is to explore the catalytic activity of a series of Co–Mo/Al_2O_3 catalysts for DRM under MW irradiation. The mechanism of the activation of Co–Mo/Al_2O_3 catalyst for DRM reaction under MW irradiation is explored. The correlation between the molar ratios of Co and Mo and the irradiated MW power levels on the catalytic activity and stability is also attempted.

2. Experimental

2.1. Catalyst preparation

The list of chemicals used in this study is shown in the ESI† (Table S1). Quartz tube reactors were purchased from Monash Scientific Glass Blowing Services, Australia. In this study, monometallic catalysts (Co_x/Al_2O_3, Mo_y/Al_2O_3) with the molar fraction of each metallic component from 0.1 to 0.6 were prepared by the conventional wet co-impregnation method. Co–Mo/Al_2O_3 bimetallic catalysts (molar fraction of Mo fixed at 0.1) with different Co/Mo molar ratios of 0.5 (CoMo0.5), 1.0 (CoMo1), 1.5 (CoMo1.5), 2.0 (CoMo2), and 2.5 (CoMo2.5) were separately prepared. Cobalt(II) nitrate and ammonium molybdate tetrahydrate were accurately weighed and properly dissolved in deionized water. The solution was stirred for 4 h. Al_2O_3 spheres (dried at 100 °C overnight to eliminate humidity) were then added into the solution and stirred for 2 h at room temperature. The precursor mixture was slowly heated up to 60 °C at a heating rate of 1 °C min^{-1} and maintained at this temperature for 12 h in the furnace. The sample was then ramped up to 250 °C for 4 h before ramping up to 600 °C and maintained at this temperature for 6 h at a heating rate of 1 °C min^{-1}.

2.2. Catalyst characterization

Powder X-ray diffraction (XRD) analysis of the catalysts was performed using the Empyrean X-ray with Cu Kα radiation (λ = 0.15418 nm) in the scan range of 10–90° with a scanning step size of 0.01° and time of 2 s. Rietveld refinement analysis was performed by using the FullProf Suite program. N_2 adsorption and Brunauer–Emmett–Teller (BET) measurements were conducted using the Tristar II 3020 equipment. The samples were degassed at 250 °C for 16 h prior to running with liquid N_2. Temperature-programmed reduction (H_2-TPR) experiments were conducted by using the ChemBET 3000 equipment. For each analysis, 0.1 g of the catalyst powder was subsequently loaded into a quartz cell. The sample was outgassed at 250 °C for 4 h with flowing N_2 through the cell to eliminate contaminants on the surface of the catalyst samples. A gas mixture of 5% H_2/N_2 at a total flow rate of 20 ml min^{-1} was induced through the quartz cell. The reduction temperature was increased from room temperature to 950 °C. The morphology of the fresh and spent catalysts were characterized by field emission scanning electron microscopy (FESEM, Zeiss NEON 40 EsB CrossBeam) equipped with energy-dispersive X-ray spectroscopy (EDX) at an acceleration voltage of 20 keV, yielding compositional and atomic dispersion analyses. Moreover, scanning transmission electron microscopy (STEM) with high-angle annular dark-field (HAADF) and bright field (BF) accompanied with the EDX detector (FEI Titan G2 80-200 TEM/STEM microscope) were employed to analyze the catalyst structure. All the STEM-EDX samples were deposited by immersing onto a copper support grid. In this work, a superconducting quantum interference device (SQUID), Quantum Design MPMS-7, was employed to evaluate the magnetic properties of the reduced catalysts with a maximal applied field of 20 kOe.

2.3. Catalytic activity measurement

The DRM catalytic activity of all the prepared catalysts were subsequently measured at atmospheric pressure using a commercial MW reactor system (Alter, SM 1150T, Canada). The schematic diagram of the DRM heated by a MW system is shown in the ESI† (Fig. S1). The output power of the MW generator can be flexibly set between 0 and 3000 W at a fixed frequency of 2.45 GHz. Two directional couplers were inserted into the microwave guide system to monitor the forwarded/reflected MW power. Prior to the DRM reaction, the calcined catalysts were subsequently reduced in a tube furnace with the mixture of 10% H_2/N_2. N_2 was first introduced through the tube furnace at 600 °C for 1 h to remove moisture and impurities in the catalysts. A gas mixture of 10% H_2/N_2 at a total flow rate of 10 mL min^{-1} was injected through the furnace for 6 h at 600 °C to reduce the catalyst samples. After reduction, the catalyst samples were maintained in an inert condition with N_2 (10 mL min^{-1}) to

5316 | Catal. Sci. Technol., 2018, 8, 5315–5324

This journal is © The Royal Society of Chemistry 2018

cool down to room temperature to prevent catalyst re-oxidation. The catalyst bed inside the quartz tube reactor (120 × 25 × 1.68 mm) was loaded with quartz wool and 4 g of fresh catalyst. The total feed flow rate fixed for all the tests was controlled at volumetric hourly space velocity (VHSV) of 10 L g^{-1} h^{-1} with CO_2/CH_4 = 1.0. For each catalytic activity measurement, the MW power was gradually increased from 50 to 1000 W at 50 W intervals. In the downstream section, the product stream was passed through a water trap to separate condensable products. The effluent gas was analyzed by gas chromatography (Agilent 7890A) equipped with two columns: (i) HP-5 connected to a MS detector for analyzing C_{2+} compounds and (ii) TDX 01 connected to a TCD detector for H_2, CO, CO_2, N_2, and CH_4 quantitative analyses. The analyses were performed after the DRM reaction was established and each analysis was repeated three times. Additional details about the reactant conversion and product selectivity calculation can be found in the ESI.†

3. Results and discussion

3.1. Catalytic activity

The reactant gas conversions of all the fresh catalyst samples were collected under steady-state conditions; the results are shown in Fig. 1.

It is noteworthy that either of the monometallic catalyst Co or Mo supported by Al_2O_3 was inactive for DRM under MW heating. Hence, no reactant conversions or syngas selectivity was detected at all the tested MW power levels from 50 to 1000 W. In contrast, the bimetallic catalysts of Co–Mo/

Al_2O_3 started to convert approximately 35% CH_4 and 47% CO_2 for CoMo0.5 and MW power of 500 W. There is another observation that the required minimum MW power level to activate the bimetallic catalysts declines with an increase in the Co loading up to Co/Mo of 2. The bimetallic catalysts of CoMo2 and CoMo2.5 could be activated at far lower MW power (200 W) than those with CoMo1 (400 W) and CoMo1.5 (300 W), respectively. Furthermore, a higher Co/Mo molar ratio value resulted in larger reactant conversion and syngas selectivity. However, both CH_4 or CO_2 conversions and H_2 or CO selectivity increased with the Co/Mo loading increase up to 2. A further addition of Co such as Co/Mo ratio of 2.5 results in a reversible effect, possibly due to the fact that the excessive amount of Co promotes the formation of inactive phases to suppress surface active sites that prevent the incident MW wave adsorption, and therefore, lowering the activity. Such influences will be discussed shortly. Notably, the conversion of CO_2 was higher than that of CH_4 and the selectivity of CO was also higher than that of H_2 for all the tested cases. Moreover, both CH_4 and CO_2 conversion increases with the MW power (Fig. 1a and b). In contrast, there are two opposite trends of H_2 and CO selectivity variation toward the employed MW power levels (Fig. 2a and b). Moreover, the selectivity of H_2 gradually declined, while that of CO sharply increased with increasing MW power, which also leads to a decrease in the syngas ratio of H_2/CO (Fig. S2†).

This observation reveals that in addition to the major DRM reaction (eqn (1)), the other reactions such as carbon deposition (eqn (2)), Boudouard reactions (eqn (3)), and
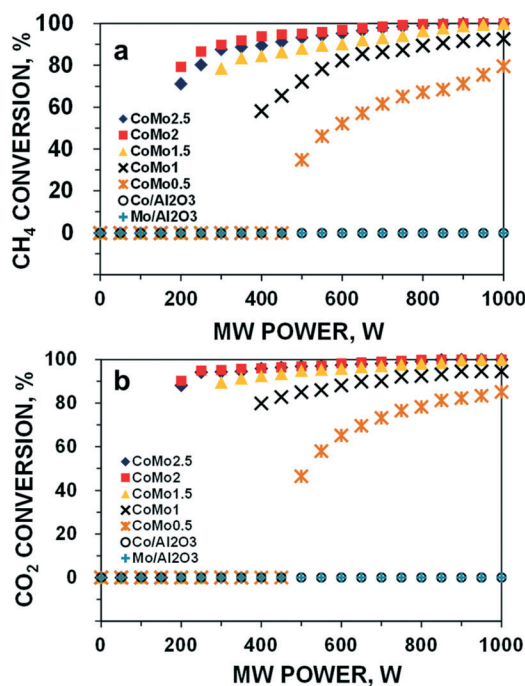

Fig. 1 CH_4 conversion (a) and CO_2 conversions (b) of DRM reaction for all the catalysts over MW irradiation at different MW power levels. Reaction parameters: CH_4/CO_2 = 1, VHSV = 10 L g^{-1} h^{-1}.
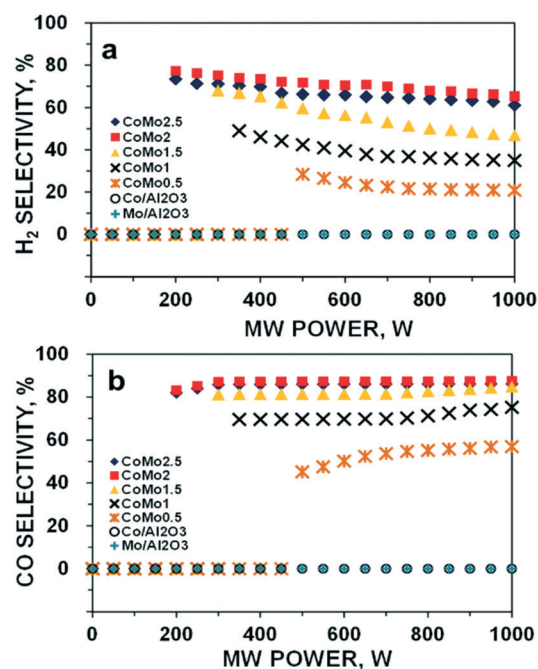

Fig. 2 H_2 selectivity (a) and CO selectivity (b) of DRM reaction for all the catalysts over MW irradiation at different MW power levels. Reaction parameters: CH_4/CO_2 = 1, VHSV = 10 L g^{-1} h^{-1}.

This journal is © The Royal Society of Chemistry 2018

Catal. Sci. Technol., 2018, **8**, 5315–5324 | **5317**

reversed water gas shift (RWGS) (eqn (4)) would simultaneously occur.

$$CH_4 + CO_2 \leftrightarrow 2H_2 + 2CO \qquad (1)$$

$$CH_4 \leftrightarrow C + 2H_2 \qquad (2)$$

$$CO_2 + C \leftrightarrow 2CO \qquad (3)$$

$$CO_2 + H_2 \leftrightarrow CO + H_2O \qquad (4)$$

Numerous papers in the literature have reported the observation of water as a byproduct of the DRM reaction.[38,39] In this work, a marginal amount of water production was observed (Fig. S1†), confirming the occurrence of the RWGS reaction (eqn (4)). The side reactions such as eqn (3) and (4) are highly endothermic,[40] and therefore, the H_2/CO ratio declined as the MW power levels increased (Fig. S2†). Furthermore, it should be noted that C is a strong MW absorber;[20] consequently, the Boudouard reaction (eqn (3)) would be further facilitated for C removal, suppressing the C residue (deposition) under MW irradiation. A similar observation was made by other researchers.[41] The incident MW radiation creates transient electron–hole pairs on the C surface, which act as radical anions and cations, reducing CO_2 molecules to generate CO. Therefore, the use of MW irradiation exhibits additional advantages: not only promoting the Boudouard reaction to produce more CO, but also reducing C deposition. However, this advantage of using MW irradiation for DRM can only be reflected in a heterogeneous catalyst system with inherent capability to absorb MW without the need of including other MW absorbers (e.g., C). Other researchers explored the catalytic performance with C (a good MW acceptor) or mixed C with more active catalysts such as Ni/Al_2O_3.[42–44] In these catalyst systems, the maximum conversions of CH_4 (>90%) and CO_2 (>80%) could be obtained at a temperature above 800 °C. However, the decrease in the catalytic activity was rapidly observed in less than 1 or 2 h. The reason for such poor stability is due to the occurrence of the Boudouard reaction (eqn (3)), leading to C loss during the DRM process.[20] Pt, a noble metal with high catalytic activity, was also mixed with active C for DRM under MW heating.[45] As reported, the amount of C catalyst was decreased over approximately 270 min at 34 mL min^{-1}, $CH_4/CO_2 = 1$, and MW power of 150 W. As compared to the reported C-based catalysts,[43] CoMo2 showed good catalytic activity, converting 80% CH_4 and 93% CO_2 to the syngas ratio (H_2/CO) of 0.80 at a higher total VHSV of 10 L g^{-1} h^{-1} and low MW power of 200 W. In addition to the higher catalytic activity, the bimetallic catalyst also exhibited better stability. The long-time tests of CoMo2 for DRM over 16 h time-on-stream (TOS) under MW irradiation with 3 typical MW power levels (200, 500, and 1000 W) were conducted, and the results are shown in Fig. 3. The catalytic performance of the tested bimetallic catalyst is almost constant over 16 TOS at MW power of 200 W. At higher MW power of 500 W, a minor decline in the catalytic
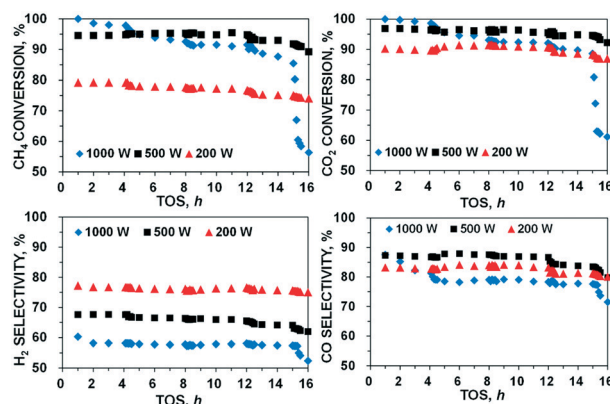

Fig. 3 Catalytic stability of CoMo2 catalyst at three different MW power levels. Reaction parameters: $CH_4 : CO_2 = 1$, VHSV = 10 L g^{-1} h^{-1}.

activity was observed. However, at MW power of 1000 W, the decline in the catalytic performance was more apparent as compared to that under lower MW. The CoMo2 catalyst delivers highly stable catalytic activity owing to its intrinsic ability to absorb MW energy without the need of mixing with C in the catalyst bed, which would lead to shorter catalyst lifetime because of C loss during the DRM reaction. Pt catalyst supported by γ-Al_2O_3 can also be activated under MW heating for DRM at the total VHSV of 7.2 L g^{-1} h^{-1}.[46] Nevertheless, such a noble metallic-based catalyst is infeasible for large-scale applications[47] due to high catalyst costs.

Other catalysts with carbonaceous material developed by Zhu and coworkers were investigated for syngas production via DRM heated by MW (350–600 W) over Ni/CeO_2 catalyst doped with Cr/Fe/Ta at total VHSV of 10.2 L g^{-1} h^{-1}.[48] In situ grown carbonaceous materials like graphene or carbon nanotubes were cleverly used to increase the MW absorption and reaction efficiency. However, the long-term stability of the catalytic performance is still a problem due to C loss. Very recently, Gangurde and coworkers synthesized Ru-doped $SrTiO_3$ perovskite catalysts that could also absorb MW energy for DRM.[49] Nonetheless, an excessive amount of CO_2 was needed to be present in the feed gas to limit C formation. This, without doubt, increases the downstream burden to separate or recycle the unreacted CO_2, leading to complexities in the DRM process.[13]

3.2. Catalyst characterization

A series of physical analyses were performed to appraise the relationship between the catalyst structure and catalytic activity for DRM under MW irradiation. The characterization results of CoMo2 bimetallic catalyst are presented with some monometallic catalysts for comparison purposes. Fig. 4A shows the N_2 absorption/desorption isotherm curves of monometallic and CoMo2 catalyst samples. As observed, the physisorption isotherm curves of both monometallic and bimetallic catalysts ascribe to type IV (Fig. 4A), which is a
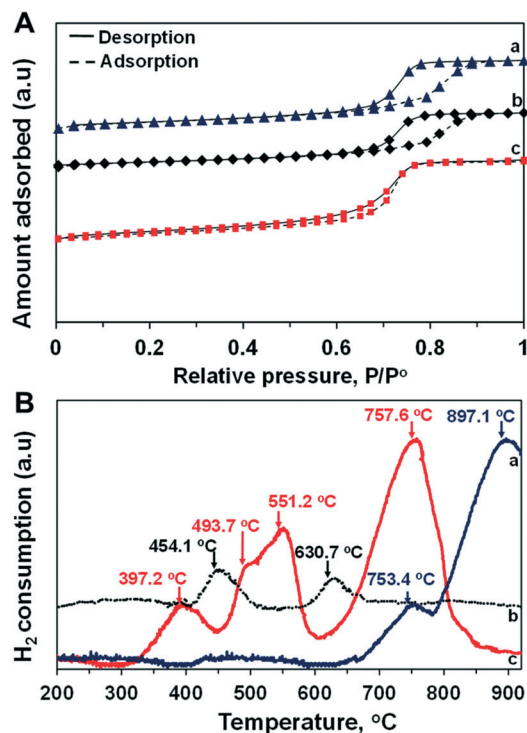
5318 | Catal. Sci. Technol., 2018, 8, 5315–5324

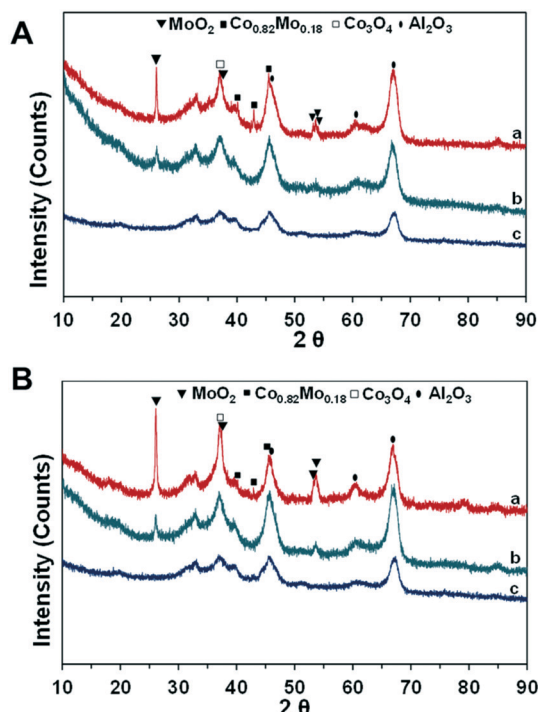This journal is © The Royal Society of Chemistry 2018

Fig. 5 XRD of fresh (A) and spent (B) catalysts: (a) CoMo2; (b) Mo/Al_2O_3; (c) Co/Al_2O_3. Reaction parameters: 500 W, $CH_4 : CO_2 = 1$, VHSV = 10 L g^{-1} h^{-1}.

Fig. 6 XRD patterns fitted using the Rietveld refinement method for the CoMo2 catalyst sample. $\chi^2 = 1.12$.

visibly detected from this bimetallic catalyst (Fig. 5). This observation displays a complex dispersion of metallic components into the support structure. It is worth noting that the diffraction peaks at 40.10°, 42.91°, and 45.48° (PDF 96-152-5121), ascribed to the $Co_{0.82}Mo_{0.18}$ bimetallic alloy, are detected from the bimetallic catalysts.

Gaytan and coworkers also observed the crystal pattern of the $Co_{0.82}Mo_{0.18}$ alloy when fabricating a Co-based alloy by the electron beam melting method.[54] The presence of this bimetallic alloy affirms the previous TPR-H_2 profile on the prediction regarding the reduction of bimetallic oxide such as $CoMoO_4$ to $Co_{0.82}Mo_{0.18}$ alloy within the range of temperatures from 490 to 555 °C. The presence of $Co_{0.82}Mo_{0.18}$ is very unique for a bimetallic catalyst and may be the reason for Co–Mo/Al_2O_3 bimetallic catalysts to be active for DRM under MW irradiation. Furthermore, the Rietveld refinement analysis result of fresh CoMo2 catalysts (Fig. 6) indicates that the cell parameters of the $Co_{0.82}Mo_{0.18}$ alloy (Table S4†) can be assigned to the space group symmetry of $P6_3/mmc$ with hexagonal crystallography ($a = 2.5582$ Å and $c = 4.2231$ Å, $\alpha = \beta = 90°$). Further, there is good matching between the XRD patterns of the CoMo2 catalyst and the calculated model, as confirmed by the graphical fitting and by the values of the agreement factor ($\chi^2 = 1.42$). After 16 h TOS of DRM reaction under MW irradiation, the crystalline structure of monometallic catalysts remained unaltered (Fig. 5B) since Co/Al_2O_3 or Mo/Al_2O_3 does not facilitate DRM under MW heating. For the spent Co–Mo/Al_2O_3 catalyst, the patterns of MoO_2, $Co_{0.82}Mo_{0.18}$, and Co_3O_4 are still detected. This result evokes

the stability of the crystalline structure of bimetallic catalysts under the redox environment of DRM reaction as well as MW irradiation, leading to enduring catalytic stability. Noticeably, the $Co_2Mo_3O_8$ phase can be visibly identified at 17.87° and 25.29° (PDF 96-152-4069) from the spent CoMo2.5 catalyst (Fig. S5b†). The appearance of the $Co_2Mo_3O_8$ phase elicits either the reaction between finely dispersed metallic Co^0 and MoO_x or the oxidation of $Co_{0.82}Mo_{0.18}$ in the oxygen-rich reforming environment.
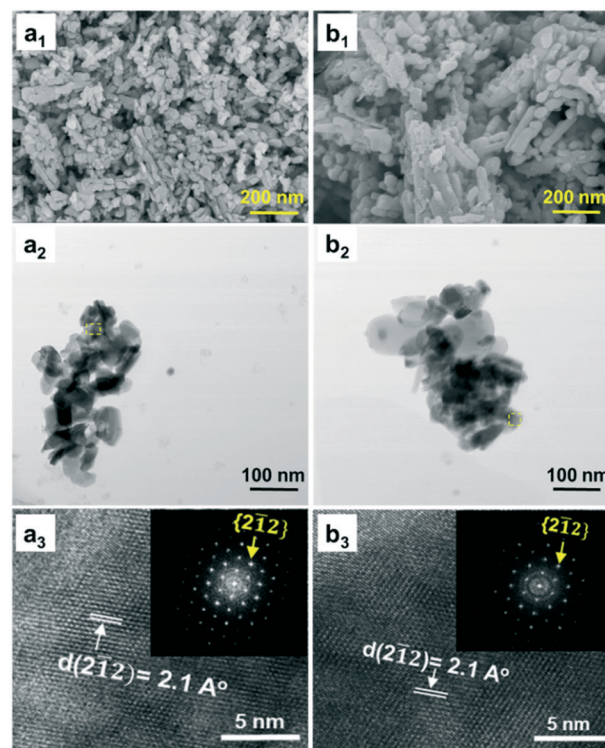
Fig. 7 FESEM (a_1 and b_1), BF-STEM, (a_2 and b_2), and HRTEM images (a_3 and b_3) of fresh (a_1–a_3) and spent (b_1–b_3) CoMo2 catalysts. Reaction parameters: 200 W, $CH_4 : CO_2 = 1$, VHSV = 10 L g^{-1} h^{-1}.

5320 | *Catal. Sci. Technol.*, 2018, **8**, 5315–5324

This journal is © The Royal Society of Chemistry 2018

The morphology of fresh CoMo2 characterized by FESEM (Fig. 7a$_1$) exhibits randomly oriented particles with relatively uniform size distribution. Moreover, its FESEM-EDX analysis results (Fig. S6†) indicate the locations that contain larger atomic numbers of both Mo and Co, reflecting the presence of Co$_{0.82}$Mo$_{0.18}$ bimetallic alloy.

Meanwhile, the FESEM-EDX images of the Co/Al$_2$O$_3$ sample (Fig. S7†) show good dispersion of Co atoms onto the support surface, which coincides with the absence of its diffraction peaks from the XRD analysis. Conversely, the MoO$_2$ particles are clearly observed from the FESEM-EDX images of the Mo/Al$_2$O$_3$ catalyst (Fig. S8†). Further, it is evident that the BF-STEM image of the fresh CoMo2 catalyst (Fig. 7a$_2$) exhibiting elongated and prismatic aggregated particles is confirmed at the nanometric scale. The HRTEM together with the corresponding fast Fourier transform (FFT) analysis for a selected area (dashed yellow squares) indicates that the bimetallic catalyst system is extensively crystalline proven by the well-arranged dots (inset, Fig. 7a$_3$). The HRTEM analysis result also reflects the interplanar distance (d_{spacing}) of 2.1 Å of the lattice plane $\{2\bar{1}2\}$ along the [110] zone axis. Unfortunately, the hexagonal atomic structure of Co$_{0.82}$Mo$_{0.18}$ bimetallic alloy could not be probed since it was effectively superimposed with other metallic species in the support leading to thicker areas, which is not appropriate for fringe lattice analyses. Alternatively, the STEM-EDX analysis can confirm the presence of this alloy. In good agreement with the abovementioned FESEM-EDX results of the fresh CoMo2 catalyst, the STEM-HAADF image (Fig. 8a), which exhibits the brightest locations containing higher atomic numbers of Co and Mo, together with the STEM-EDX results further (Fig. 8c) consolidate the presence of the bimetallic alloy on the support surface.
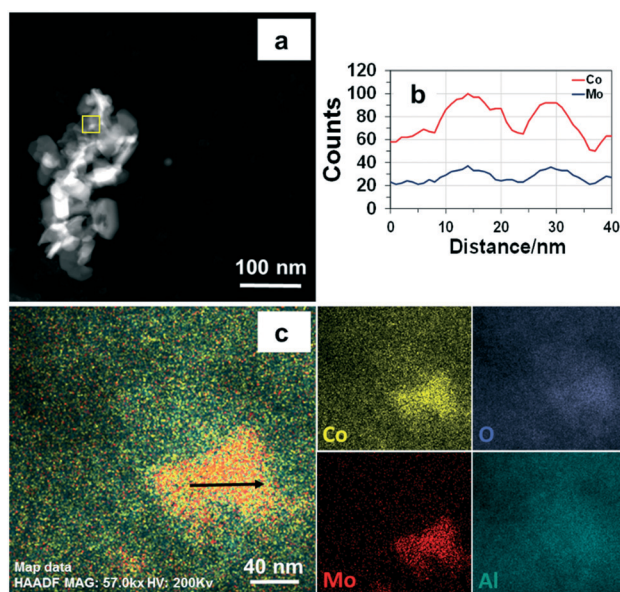

Fig. 8 STEM-HAADF (a), line-scanning signals (b), and STEM-EDX (c) images of fresh CoMo2 catalyst.

Moreover, as shown from the line-scanning analysis (Fig. 8b), the Co and Mo signals are visibly detected. The line-scanning analysis is in good accordance with the nanoscale mapping results (Fig. 8c). This reveals that the Co and Mo components are overlaid on each other, revealing the presence of the Co$_{0.82}$Mo$_{0.18}$ bimetallic alloy. In the meantime, the STEM-EDX qualitative spectrum of fresh CoMo2 catalyst (Fig. S10†) confirms all the constitutive elements, i.e., Co, Mo, O, and Al. The unlabeled peaks belong to the Cu grid. For the spent CoMo2 catalyst, insignificant sintering of particles was observed from the catalyst surface (Fig. 7b$_1$), revealing the physical stability of the bimetallic catalyst. Likewise, all the STEM analysis results of the spent CoMo2 catalyst (Fig. 7b$_2$ and b$_3$ and S11†) confirm the stability of the crystal structure of the bimetallic catalyst that was maintained after 16 h on stream test under MW irradiation at MW power of 500 W. All these observed results, therefore, validate the stability of the bimetallic catalyst structure under MW irradiation. However, the previous long-time tests indicate a reduction in the catalytic activity at high MW power levels (e.g., 500 and 1000 W). Hence, the FESEM analyses at different magnifications for the spent CoMo2 catalyst samples tested under different MW power levels (200, 500, and 1000 W) were performed, and the results (Fig. S9†) exhibit visible sloughing and distortion on the CoMo2 surface after 16 h on stream of the DRM reaction under MW irradiation at 500 W. These deteriorations are particularly serious at higher MW power levels (e.g., 1000 W). On the other hand, at low MW power (e.g., 200 W) in which the CoMo2 catalyst can yield relatively higher reactant gas conversions (80% CH$_4$ and 93% CO$_2$), no visibly distinguishable differences are observed in the morphology between the fresh and spent catalyst samples. Hence, the outer physical deterioration would be the principal reason for the abovementioned decrease in the catalytic activity at higher MW power levels, as shown in Fig. 3. It is noteworthy that no sign of coke deposition could be observed from the spent CoMo2 catalyst (Fig. S10†). It is possible that the carbonaceous-free observation from the spent bimetallic catalyst is due to the mentioned Boudouard reaction promoted by MW irradiation to form more CO. The STEM-EDX qualitative spectrum also indicates the absence of C-related peaks from the spent CoMo2 catalyst (Fig. S12†). Positively, the catalytic DRM reaction driven by MW irradiation can assist in reducing the deposited coke and delivering higher catalytic activity.

3.3. Mechanism of catalytic activation for DRM under MW irradiation

Despite the fact that some research works have reported about catalytic DRM processes under MW heating, the activation mechanism of metallic-based catalysts by MW irradiation has not been fully understood. This is due to the fact that almost all the reported works either utilize C as the catalyst or mix metallic-based catalysts with a good MW absorber, i.e., C for DRM reaction under MW heating. This study

This journal is © The Royal Society of Chemistry 2018

Catal. Sci. Technol., 2018, 8, 5315–5324 | 5321

explored that the Co–Mo/Al_2O_3 catalyst can directly absorb MW radiation and exhibit high catalytic activity for DRM, while their monometallic counterparts are inactive. The XRD results indicate the presence of $Co_{0.82}Mo_{0.18}$ alloy in bimetallic catalysts, which are distinguishable from monometallic catalyst samples. Therefore, from this observation, we can understand that the $Co_{0.82}Mo_{0.18}$ alloy is the MW acceptor component, which absorbs MW energy leading to heating the catalyst and catalyzing the DRM reaction. Indeed, it is generally recognized that magnetodielectric materials that simultaneously possess ferromagnetic and dielectric properties are the best MW absorbers.[55–58] Co, known as a ferromagnetic element,[59] can combine with other paramagnetic metals such as Mo (ref. 60) to form magnetodielectric materials for MW-absorbing applications.[61] In this study, the magnetic properties as a function of the magnetic field of the prepared catalysts were measured by using SQUID. The results are shown in Fig. 9. The previous XRD patterns of the Co/Al_2O_3 catalyst indicate the absence of a Co-based diffraction pattern, which can be explained by the effective dispersion of Co-based particles in the support structure (Fig. S6†). However, it can be observed that the saturated magnetization is in the order of Co/Al_2O_3 > CoMo2 > Mo/Al_2O_3. The Co/Al_2O_3 catalyst exhibits a small M–H (magnetic moment–magnetic field) loop (Fig. 9), which is a representative feature for these soft ferromagnetic materials to absorb MW radiation. Consequently, the presence of well-dispersed metallic particles into the support can also effectively absorb the incident MW radiation.[62,63] However, in this work, the Co/Al_2O_3 catalyst could not absorb MW energy presumably because of its high electrical conductivity, which causes the large reflection of the incident MW radiation.[64]

The Mo/Al_2O_3 catalyst exhibited low magnetic characteristics (Fig. 9), limiting the ability to couple with the incident MW radiation.[65] Hence, Mo/Al_2O_3 could not absorb MW energy. In the mixture of Co and Mo, conversely, the resultant Co–Mo/Al_2O_3 catalyst possesses higher saturated magnetization as compared to Mo/Al_2O_3 (Fig. 9).
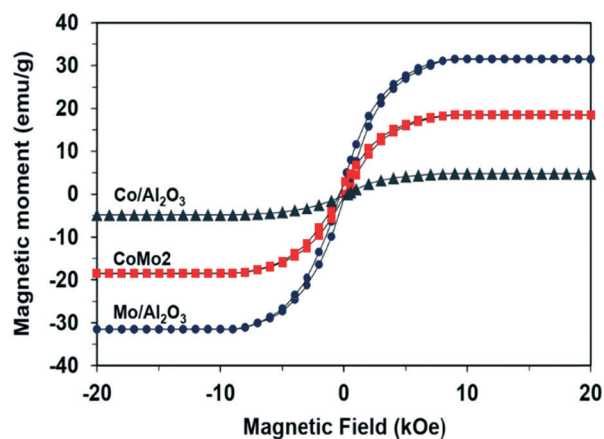
Although it possesses lower saturated magnetization than Co/Al_2O_3, CoMo2 still exhibits the characteristics of a soft ferromagnetic material (small M–H loop), which is able to couple with the incident MW radiation.[58,66] Therefore, Co–Mo/Al_2O_3 bimetallic catalysts in the presence of $Co_{0.82}Mo_{0.18}$ possessing magnetodielectric properties promote MW energy acceptance, which leads to its heating up to catalyze the DRM reaction. Under this situation, the $Co_{0.82}Mo_{0.18}$ alloy itself has a dual function in which it can serve as a MW-absorbing component and an active center for the DRM reaction. This mechanism is in good agreement with the other researchers[65,67] who have also indicated that the best MW absorbers contain one of the phases responsible for coupling with electromagnetic waves, while the other works as an insulator to localize MW energy conversion.

As per the literature, both Co/Al_2O_3 and Mo/Al_2O_3 exhibit its catalytic activity for DRM under conventional heating. In these works, Co-based[28] and Mo-based particles[30] act as active centers for DRM reactions. Meanwhile, it is hypothesized that MW heating can generate internal heat sources for heterogeneous catalysts, which have inherent MW-absorbing capability.[13] In this situation, the heated $Co_{0.82}Mo_{0.18}$ alloy can be considered as an internal heat source to simultaneously heat up adjacent metals, i.e., well-dispersed Co^0, or metallic oxides, i.e., Co_3O_4 and MoO_2, due to its effective dispersion with other components in the support, as shown in the FESEM-EDX and STEM-EDX results. The formation of these extra active centers results in the tremendous increase in the reactant conversions when reaching an initially active MW power level before exhibiting a gradually and slowly increasing rate with a subsequent increase in the MW power levels (Fig. 1). In particular, Co-based particles are well known as effective active centers for DRM reactions.[68] By introducing additional auxiliary active centers under MW heating, the catalytic activity and stability of Co/Mo-supported Al_2O_3 catalysts was effectively preserved over 16 h TOS of DRM at low MW powers (Fig. 3), regardless of the observed reduction in the porosity as indicated by the previous BET analyses. Nonetheless, an excessive Co molar loading (e.g., Co/Mo ratio of 2.5) possibly either leads to an increase in the electrical conductivity (generated by the additional reduced Co particles) or promotes the formation of the abovementioned inactive phases such as $Co_2Mo_3O_8$ (Fig. S5†), smothering the active centers from the incident MW radiation. These two consequences engender the reduction in the MW-absorbing capability, and therefore, diminish the catalytic activity.

Conclusions

In this work, the catalytic activity of a series of Co- and Mo-based catalysts supported by Al_2O_3 for DRM under MW irradiation at the ambient pressure were explored. As compared to the reported previous works focusing on C-containing catalysts, the Co–Mo/Al_2O_3 catalyst with Co/Mo molar ratio of 2 delivered higher activity and stability for DRM converting CH_4 (80%) and CO_2 (93%) to the syngas with H_2/CO ratio of

Fig. 9 Hysteresis loops of the curves of fresh Mo/Al_2O_3, Co/Al_2O_3, and CoMo2 catalysts.

5322 | Catal. Sci. Technol., 2018, 8, 5315–5324

This journal is © The Royal Society of Chemistry 2018

0.80 under lower MW irradiation power of 200 W. Our results highlight the high activity of the bimetallic catalyst attributed to the MW-absorbing ability of the $Co_{0.82}Mo_{0.18}$ alloy combining the ferromagnetic and dielectric properties. The developed bimetallic catalyst exhibited an intrinsic ability to absorb MW energy without the involvement of extra MW acceptors such as C-based materials, leading to better catalytic stability. There is no significant sign for catalyst decay during the 16 h stability test at low MW power levels (<500 W). The MW-heated DRM process over $Co–Mo/Al_2O_3$ catalyst in this study is flexible and relocatable, and therefore, appropriate for FPSOV systems to efficiently use these remote and stranded gas reserves *via* the Fischer–Tropsch synthesis.

Conflicts of interest

There are no conflicts to declare.

Acknowledgements

Notes and references

1 W. Hoppe, S. Bringezu and N. Thonemann, *J. Cleaner Prod.*, 2016, **121**, 231–237.
2 J.-M. Lavoie, *Front. Chem.*, 2014, **2**, 81.
3 H. Meng, L. Kloul and A. Rauzy, *Appl. Ocean Res.*, 2018, **74**, 117–126.
4 M. Ao, G. H. Pham, V. Sage and V. Pareek, *J. Mol. Catal. A: Chem.*, 2016, **416**, 96–104.
5 A. Löfberg, J. Guerrero-Caballero, T. Kane, A. Rubbens and L. Jalowiecki-Duhamel, *Appl. Catal., B*, 2017, **212**, 159–174.
6 M. Usman, W. M. A. Wan Daud and H. F. Abbas, *Renewable Sustainable Energy Rev.*, 2015, **45**, 710–744.
7 J. Menéndez, A. Arenillas, B. Fidalgo, Y. Fernández, L. Zubizarreta, E. Calvo and J. Bermúdez, *Fuel Process. Technol.*, 2010, **91**, 1–8.
8 D. Varisli, C. Korkusuz and T. Dogu, *Appl. Catal., B*, 2017, **201**, 370–380.
9 J.-Q. Zhang, Y.-J. Yang, J.-S. Zhang and Q. Liu, *Acta Chim. Sin.*, 2002, **60**, 1973–1980.
10 T.-S. Kim, S. Song, K.-M. Chun and S. H. Lee, *Energy*, 2010, **35**, 2734–2743.
11 M. Jasiński, M. Dors and J. Mizeraczyk, *J. Power Sources*, 2008, **181**, 41–45.
12 X. Tao, M. Bai, X. Li, H. Long, S. Shang, Y. Yin and X. Dai, *Prog. Energy Combust. Sci.*, 2011, **37**, 113–124.
13 A. Dastan, A. Kulkarni and B. Torok, *Green Chem.*, 2012, **14**, 17–37.
14 B. Fidalgo and J. A. Menéndez, *Fuel Process. Technol.*, 2012, **95**, 55–61.
15 B. Fidalgo, A. Domínguez, J. J. Pis and J. A. Menéndez, *Int. J. Hydrogen Energy*, 2008, **33**, 4337–4344.
16 A. Domínguez, Y. Fernández, B. Fidalgo, J. J. Pis and J. A. Menéndez, *Energy Fuels*, 2007, **21**, 2066–2071.
17 B. Fidalgo, A. Arenillas and J. A. Menéndez, *Fuel*, 2010, **89**, 4002–4007.
18 L. Li, Z. Yang, J. Chen, X. Qin, X. Jiang, F. Wang, Z. Song and C. Ma, *Fuel*, 2018, **215**, 655–664.
19 L. Li, H. Wang, X. Jiang, Z. Song, X. Zhao and C. Ma, *Fuel*, 2016, **185**, 692–700.
20 J. A. Menéndez, A. Arenillas, B. Fidalgo, Y. Fernández, L. Zubizarreta, E. G. Calvo and J. M. Bermúdez, *Fuel Process. Technol.*, 2010, **91**, 1–8.
21 V. R. R. Pendyala, W. D. Shafer, G. Jacobs, M. Martinelli, D. E. Sparks and B. H. Davis, *RSC Adv.*, 2017, **7**, 7793–7800.
22 B. V. Ayodele, S. S. Hossain, S. S. Lam, O. U. Osazuwa, M. R. Khan and C. K. Cheng, *J. Nat. Gas Sci. Eng.*, 2016, **34**, 873–885.
23 B. V. Ayodele, M. R. Khan, S. S. Lam and C. K. Cheng, *Int. J. Hydrogen Energy*, 2016, **41**, 4603–4615.
24 N. A. Abd Ghani, A. Azapour, A. F. a. Syed Muhammad and B. Abdullah, *Int. J. Hydrogen Energy*, 2018, 1–8, in press.
25 B. V. Ayodele, M. R. Khan and C. K. Cheng, *Int. J. Hydrogen Energy*, 2016, **41**, 198–207.
26 O. Marin-Flores, T. Turba, C. Ellefson, K. Wang, J. Breit, J. Ahn, M. G. Norton and S. Ha, *Appl. Catal., B*, 2010, **98**, 186–192.
27 A. E. Awadallah, A. A. Aboul-Enein and A. K. Aboul-Gheit, *Energy Convers. Manage.*, 2014, **77**, 143–151.
28 J. L. Ewbank, L. Kovarik, C. C. Kenvin and C. Sievers, *Green Chem.*, 2014, **16**, 885–896.
29 É. Horváth, K. Baán, E. Varga, A. Oszkó, Á. Vágó, M. Törő and A. Erdőhelyi, *Catal. Today*, 2017, **281**, 233–240.
30 M. Gaillard, M. Virginie and A. Y. Khodakov, *Catal. Today*, 2017, **289**, 143–150.
31 M. Li, H. Li, F. Jiang, Y. Chu and H. Nie, *Catal. Today*, 2010, **149**, 35–39.
32 S. A. Ali, S. Ahmed, K. W. Ahmed and M. A. Al-Saleh, *Fuel Process. Technol.*, 2012, **98**, 39–44.
33 W. Chen, X. Long, M. Li, H. Nie and D. Li, *Catal. Today*, 2017, **292**, 97–109.
34 H. K. Kim, C.-W. Lee, M. Kim, J. H. Oh, S. A. Song, S.-C. Jang, C. W. Yoon, J. Han, S. P. Yoon, S. W. Nam, D.-K. Choi, Y.-g. Shul and H. C. Ham, *Int. J. Hydrogen Energy*, 2016, **41**, 18846–18857.
35 P. A. Nikulshin, A. V. Mozhaev, A. A. Pimerzin, V. V. Konovalov and A. A. Pimerzin, *Fuel*, 2012, **100**, 24–33.
36 N. M. Maximov, N. N. Tomina, P. S. Solmanov and A. A. Pimerzin, *Russ. J. Appl. Chem.*, 2017, **90**, 574–581.
37 S. J. Ardakani, M. Alyani and K. J. Smith, *Can. J. Chem. Eng.*, 2016, **94**, 655–661.
38 C. Egawa, *J. Catal.*, 2018, **358**, 35–42.
39 D. Liu, X. Y. Quek, W. N. E. Cheo, R. Lau, A. Borgna and Y. Yang, *J. Catal.*, 2009, **266**, 380–390.
40 N. Abdel Karim Aramouni, J. Zeaiter, W. Kwapinski and M. N. Ahmad, *Energy Convers. Manage.*, 2017, **150**, 614–622.
41 J. Hunt, A. Ferrari, A. Lita, M. Crosswhite, B. Ashley and A. E. Stiegman, *J. Phys. Chem. C*, 2013, **117**, 26871–26880.
42 B. Fidalgo, A. Arenillas and J. A. Menéndez, *Fuel Process. Technol.*, 2011, **92**, 1531–1536.

43 L. Li, X. Jiang, H. Wang, J. Wang, Z. Song, X. Zhao and C. Ma, *J. Anal. Appl. Pyrolysis*, 2017, **125**, 318–327.

44 L. M. Kustov, A. L. Tarasov, O. P. Tkachenko and G. I. Kapustin, *Ind. Eng. Chem. Res.*, 2017, **56**, 13034–13039.

45 L. S. Gangurde, G. S. J. Sturm, T. J. Devadiga, A. I. Stankiewicz and G. D. Stefanidis, *Ind. Eng. Chem. Res.*, 2017, **56**, 13379–13391.

46 X. Zhang, C. S.-M. Lee, D. M. P. Mingos and D. O. Hayward, *Catal. Lett.*, 2003, **88**, 129–139.

47 I. V. Zagaynov, A. S. Loktev, A. L. Arashanova, V. K. Ivanov, A. G. Dedov and I. I. Moiseev, *Chem. Eng. J.*, 2016, **290**, 193–200.

48 T. Odedairo, J. Ma, J. Chen, S. Wang and Z. Zhu, *J. Solid State Chem.*, 2016, **233**, 166–177.

49 L. S. Gangurde, G. S. J. Sturm, M. J. Valero-Romero, R. Mallada, J. Santamaria, A. I. Stankiewicz and G. D. Stefanidis, *Chem. Eng. Process.*, 2018, **127**, 178–190.

50 W. Li, J. Liu and D. Zhao, *Nat. Rev. Mater.*, 2016, **1**, 16023.

51 Z. Ferencz, A. Erdőhelyi, K. Baán, A. Oszkó, L. Óvári, Z. Kónya, C. Papp, H. P. Steinrück and J. Kiss, *ACS Catal.*, 2014, **4**, 1205–1218.

52 J. Ji, X. Duan, G. Qian, X. Zhou, G. Tong and W. Yuan, *Int. J. Hydrogen Energy*, 2014, **39**, 12490–12498.

53 B. Wang, Y. Yang, L.-J. Li and Y. Chen, *J. Mater. Sci.*, 2009, **44**, 3285–3295.

54 S. M. Gaytan, L. E. Murr, E. Martinez, J. L. Martinez, B. I. Machado, D. A. Ramirez, F. Medina, S. Collins and R. B. Wicker, *Metall. Mater. Trans. A*, 2010, **41**, 3216–3227.

55 Y. Khani, Z. Shariatinia and F. Bahadoran, *Chem. Eng. J.*, 2016, **299**, 353–366.

56 S. Das, G. C. Nayak, S. K. Sahu, P. C. Routray, A. K. Roy and H. Baskey, *J. Magn. Magn. Mater.*, 2015, **377**, 111–116.

57 X. Li, J. Feng, Y. Du, J. Bai, H. Fan, H. Zhang, Y. Peng and F. Li, *J. Mater. Chem. A*, 2015, **3**, 5535–5546.

58 A. Maqsood and K. Khan, *J. Alloys Compd.*, 2011, **509**, 3393–3397.

59 N. Tsyntsaru, H. Cesiulis, E. Pellicer, J.-P. Celis and J. Sort, *Electrochim. Acta*, 2013, **104**, 94–103.

60 C. D. Brondino, M. G. Rivas, M. J. Romão, J. J. Moura and I. Moura, *Acc. Chem. Res.*, 2006, **39**, 788–796.

61 V. Petrov and V. Gagulin, *Inorg. Mater.*, 2001, **37**, 93–98.

62 N. Clark, N. Jones and A. Porch, *Sens. Actuators, A*, 2017, **259**, 137–143.

63 C. Wang, R. Lv, Z. Huang, F. Kang and J. Gu, *J. Alloys Compd.*, 2011, **509**, 494–498.

64 R. R. Mishra and A. K. Sharma, *Composites, Part A*, 2016, **81**, 78–97.

65 S. Horikoshi and N. Serpone, *Catal. Sci. Technol.*, 2014, **4**, 1197–1210.

66 L. M. Kustov and I. M. Sinev, *Russ. J. Phys. Chem. A*, 2010, **84**, 1676–1694.

67 D. E. Clark, D. C. Folz and J. K. West, *Mater. Sci. Eng., A*, 2000, **287**, 153–158.

68 H. Ay and D. Üner, *Appl. Catal., B*, 2015, **179**, 128–138.

5324 | *Catal. Sci. Technol.*, 2018, **8**, 5315–5324

This journal is © The Royal Society of Chemistry 2018